Journal of Animal & Plant Sciences, 35(2): 2025, Page: 415-428
ISSN (print): 1018-7081; ISSN (online): 2309-8694
https://doi.org/10.36899/JAPS.2025.2.0035

MECHANISM OF PUERARIN-POLYBUTYL CYANOACRYLATE NANOPARTICLES ON APOPTOSIS OF BRAIN CELLS IN RATS WITH CARDIAC ARREST/CARDIOPULMONARY RESUSCITATION

X. Zhao*, Y.S. Xu, and J.Y. Fang

Department of Emergency, Affiliated Hangzhou First People's Hospital, Zhejiang University School of Medicine, Hangzhou, 310006, Zhejiang, China.
*Corresponding author's email: zhaoxuezjuh@163.com

ABSTRACT

Following cardiac resuscitation, cerebral perfusion pressure increases, accompanied by impaired autoregulation of cerebral blood vessels, which subsequently leads to cerebral reperfusion congestion and resultant brain injury. This study aimed to explore the therapeutic mechanism of puerarin (PARI) nanoparticles (NPs) on cardiopulmonary resuscitation after cardiac arrest in rats. PARI-polybutyl cyanoacrylate NPs (PARI-BCA-NPs) were fabricated using PARI as the model drug. While the NPs were physically characterized, the pharmacokinetics and tissue distribution of the intravenously administered drug in rats were studied. Subsequently, a rat cardiac arrest/cardiopulmonary resuscitation (CA/CPR) model was established to evaluate the protective effect of the nanodrug on brain cells. At the same dose, injection of the PARI-BCA-NP solution significantly altered the pharmacokinetic properties, increasing the mean drug retention time, blood concentration, and area under the curve (AUC) by 54% compared to the PARI injection (P<0.05). Relative to the PARI injection group, the AUC of each tissue injected with PARI-BCA-NP solution was increased drastically, and the AUC of the brain tissue injected with the NP solution was 2.72 times that of the brain tissue injected with the PARI parent drug group. Based on the CA/CPR model, rats were grouped (sham operation group, model group, and NP group). The fluorescence intensities of superoxide dismutase (SOD)1 and SOD2 in the NP group at each time point were markedly increased versus the model group (P<0.05), and positive rates of TUNEL and Caspase3/TUNEL were decreased, i.e., the apoptosis rate of brain cells was decreased (P<0.05). PARI-BCA-NPs exhibit excellent pharmacokinetic properties and significantly improve brain injury caused by CA/CPR by reducing oxidative stress and neuronal apoptosis in brain tissue. They demonstrate promising therapeutic potential in animal models, particularly in the intervention of brain injury following CA. Further research will help explore their applicability, especially their feasibility in acute-phase treatment, offering a novel therapeutic strategy.

Keywords: puerarin; PARI-BCA-NPs; pharmacokinetics; brain cell apoptosis.

Published first online February 22, 2025 Published final April 28, 2025

INTRODUCTION

Cardiac arrest (CA) and cardiopulmonary resuscitation (CPR) are critical emergencies with extremely high mortality rates, particularly post-CA brain injury (PCAI), which is a key factor contributing to patient death and long-term functional impairment. Although CPR can restore cardiac and respiratory functions, subsequent brain injury often leads to irreversible neurological damage, severely affecting patient prognosis. During cerebral ischemia-reperfusion, mechanisms such as apoptosis, oxidative stress, inflammatory responses, and blood-brain barrier (BBB) disruption interact, resulting in widespread neuronal cell death (Cheng *et al.,* 2024). Therefore, effectively mitigating brain injury after CA has become a significant research focus in the fields of emergency medicine and neuroscience.

Nanoparticles (NPs), as a novel drug delivery system, have gained significant attention in recent years due to their small particle size, good biocompatibility, easily adjustable surface properties, and ability to cross the BBB (Hoffmann *et al.,* 2019). These advantages make NPs a promising tool for targeted drug therapy. NPs can encapsulate drugs and deliver them to the brain through specific mechanisms, thereby effectively enhancing therapeutic efficacy and reducing side effects (Gvoic *et al.,* 2021). Compared to traditional drug delivery methods, NPs significantly improve targeting and bioavailability, showing immense potential, especially in the treatment of brain diseases and brain injuries (Matalqah *et al.,* 2020). However, despite some studies reporting the application of NPs in brain drug delivery (Mitchell *et al.,* 2021; Reker *et al.,* 2021), the

targeting and therapeutic efficacy of specific drug carrier systems, such as PARI-loaded polybutyl cyanoacrylate (BCA) NPs (PARI-BCA-NPs) in the treatment of post-CA brain injury, remains underexplored.

BCA NPs are a widely studied class of drug delivery systems. BCA NPs exhibit excellent biodegradability, low toxicity, and low immunogenicity, enabling effective crossing of the BBB and showing promising potential in the treatment of various brain diseases (Jahansooz *et al.,* 2020; Sønstevold *et al.,* 2021; Lott *et al.,* 2021). These properties make BCA NPs an ideal carrier for brain-targeted drug delivery, particularly in the treatment of brain ischemia, brain tumors, and neurodegenerative diseases, where significant progress has been made (You *et al.,* 2019; Sønstevold *et al.,* 2021). Furthermore, the ability of BCA NPs to penetrate the BBB and their low cellular toxicity position them as a potential strategy for treating post-CA brain injury. However, the specific mechanisms underlying the action of BCA NPs in post-CA brain injury have not yet been sufficiently explored in the existing literature.

Puerarin (PARI), a plant-derived flavonoid compound, exhibits significant pharmacological effects, including antioxidant, anti-inflammatory, anti-platelet aggregation, and microcirculation-improving activities, and is widely used in the clinical treatment of cardiovascular and cerebrovascular diseases (Zhou *et al.,* 2020; Ferraris *et al.,* 2020). PARI has demonstrated favorable therapeutic effects in the treatment of heart disease and cerebrovascular disorders, as it can alleviate oxidative stress and inflammatory responses, thereby protecting neuronal cells from damage (Zhang *et al.,* 2019; Sharma *et al.,* 2019). Recent studies showed that PARI inhibits apoptosis and improves cerebral microcirculation, particularly exhibiting promising neuroprotective effects in a rat model of cerebral ischemia-reperfusion (Chen *et al.,* 2021; Masoudi *et al.,* 2020). However, despite the broad reporting of these effects, its potential in the treatment of brain injury following CA remains insufficiently investigated.

Although there has been some progress in the application of NPs in the treatment of brain injury, research specifically focusing on the targeting properties and mechanisms of PARI-BCA-NPs in post-CA brain injury is still limited. Therefore, the aim of this study was to load PARI onto BCA NPs and administer them via intravenous injection in a rat model of CA/CPR. This study aimed to investigate the targeting ability of PARI-BCA NPs in post-CA brain injury and analyze their potential mechanisms in inhibiting neuronal apoptosis. Through this research, we aimed to fill the existing gap in the literature and provide a theoretical basis for the clinical application of PARI-BCA NPs as a novel therapeutic strategy.

MATERIALS AND METHODS

Fabrication of PARI-BCA-NPs: To prepare PARI-BCA-NPs, the one-step preparation methodology (Vimalnath *et al*., 2024) was used. The pH of the whole reaction system was set to 2, and the total volume was set to 10 mL. The choice of pH 2 was to enhance the interaction between the surfactant and the drug extract, thereby improving the emulsification efficiency and stability of the NPs, while avoiding potential issues of surfactant inactivation or drug degradation that could occur under high pH conditions. Dextran-70 (Sigma-Aldrich Corporation, USA) and Pluronic F68 (Sigma-Aldrich Corporation, USA) were configured as surfactants according to the concentration of 1: 1, The selection of these two surfactants was based on their good biocompatibility and ability to effectively reduce NP aggregation. Dextran-70 has good water solubility and biodegradability, while Pluronic F68, known for its strong stability and excellent interfacial activity, is commonly used in drug delivery systems. It can effectively stabilize the NP morphology and reduce cellular toxicity. Thirty milligrams of Radix Puerariae extract (PARI, Nanjing Zerun Pharmaceutical Co., Ltd., China) were prepared. The unit dosage of alpha-polybutyl cyanoacrylate (BCA, Beijing Shunkang Medical Adhesive Co., Ltd., China) was set at 0.6%. The conditions for configuring the ETS-D4 type timed constant temperature magnetic stirrer (IKA GmbH, Germany) were established, with the emulsification temperature set to 25°C, the stirring speed set to 500 r/min, and the stirring time set to 4 hours. Specifically, 30 mg of PARI was dissolved in a hydrochloric acid solution containing Pluronic F68 and Dextran-70 (1:1). The volume of the mixed solution was adjusted to 10 mL, and 100 μL of BCA monomer was slowly added at 25°C and 500 r/min. The pH of the solution was adjusted to 6.7 with NaOH solution (Sigma-Aldrich Corporation, USA) after stirring for 4 h, then the stirring was continued for 1 h. After filtration, a white opalescent colloid (PARI-BCA-NPs) solution was obtained.

Animal model construction and grouping: Fifty-four adult Sprague Dawley rats (Kaixue Biotechnology Co., Ltd., China) were fasted for 12 hours before the procedure, but water was allowed. Prior to surgery, each rat was intraperitoneally injected with 3% sodium pentobarbital (Foshan Chemical Experiment Factory, China) at a dose of 30 mg/kg for anesthesia. The skin was prepared and sterilized, followed by endotracheal intubation, which was then connected to a ventilator (Aokangte Instrument Co., Ltd., China) in the surgical area. Then, the left femoral artery and vein were removed by blunt dissection (Ma *et al*., 2021), and a 5 U/mL sodium heparin injection (Shandong Laiyang Biochemical Pharmaceutical Factory, China) indwelling

tube was preimplanted. A femoral indwelling catheter was connected to the BL-420F pressure sensor (Chengdu Taimeng Software Co., Ltd., China) for biological function testing, including monitoring of blood pressure and the recording of chest II ECG.

Ventricular fibrillation was induced in the rat hearts via transesophageal alternating current stimulation and continuous rapid pacing, with the voltage set at 15–25 V, pulse width at 10 ms, and frequency at 30 Hz. The criteria for successful establishment of the global cerebral ischemia–reperfusion injury (IRI) model included the following: (1) blood pressure monitoring indicating a mean arterial pressure of < 10 mmHg, and (2) the ECG showing a straight line or a small amplitude tremor, which may be due to ECG activity but no palpable pulse. CPR was performed 5 minutes after CA to restore spontaneous circulation. The criteria for recovery of spontaneous circulation were as follows: (1) supraventricular rhythm (including atrial, sinus, and bounded rhythm) occurred and (2) mean arterial pressure exceeded 20 mmHg for 2 min. Immediately after the recovery of spontaneous circulation, rats in the intervention group were injected with PARI-BCA-NPs (10 mg/kg), while rats in the control group were injected with an equal volume of normal saline. Rats in the sham operation group underwent the procedure without receiving any additional treatments. After hemodynamic monitoring for more than 1 hour, the rats were returned to their cages for further care. All rats were randomly assigned to three groups: sham operation group (Sham), model group (Model 1) and administration group (PARI-BCA-NP group). The protocols and procedures were approved by Animal Experimentation Ethics Committee of Affiliated Hangzhou First People's Hospital. The animal experiments were conducted in accordance with the relevant provisions the Chinese Association for Laboratory Animal Sciences.

Physical characterization of PARI-BCA-NPs: According to the obtained optimized preparation suspension, an appropriate amount of the suspension was ingested, diluted 10 times, transferred to a copper mesh (EM Resolutions, UK), added to 2% phosphotungstic acid (Sigma-Aldrich, USA) for secondary staining, and dried. The morphology of the prepared particles was visualized by Hitachi H-7000 Transmission Electron Microscope (Hitachi Corporation, Japan). A certain amount of the PARI-n-butyl cyanoacrylate solution, prepared by the optimized process, was placed in a laser particle size analyzer to determine the particle size and its distribution. The existing form of PARI in the NPs was analyzed using a DSC 5+ differential scanning calorimeter (Mettler-Toledo Technology Co., Ltd., China). PARI, the blank NP lyophilized product, and 10 mg of PARI-BCA-NPs were analyzed for comparison. With Al_2O_3 (Alcoa Corporation, USA) as the reference, each sample was subjected to DSC analysis with a scanning rate of 10°C/min, a scanning range of 30–400°C and a N_2 flow rate of 0.2 mL/min.

The interaction between the BCA monomer and drug in the polymerization was analyzed using FTIR-650 Fourier transform infrared spectrometer (Tianjin Gangdong Technology Co., Ltd., China). Next, 1 mg of BCA monomer, 1 mg of PARI, 1 mg of the blank NP lyophilized product, and 1 mg of the PARI-BCA-NP lyophilized product were purified with potassium bromide and mixed in a mortar at ambient temperature and humidity (less than 50%). After infrared drying, the samples were compressed into pellets and placed in the optical path of the spectrometer for analysis.

Grouping and sampling methods of pharmacokinetics in rats after intravenous injection of PARI NPs: In the pharmacokinetic experiments of PARI NPs (NPs), 132 Sprague Dawley rats (half males and half females) were selected and randomly assigned to two groups. The rats were fasted for 12 hours but had free access to water before drug administration. At each time point, PARI injection and PARI-BCA-NPs were intravenously administered at a dose of 10 mg/kg to six rats in each group.

At the set time points after drug administration (PARI group: 1 min, 5 min, 10 min, 30 min, 45 min, 1 h, 2 h, 4 h, and 8 h; PARI-BCA-NP preparation group: 1 min, 5 min, 10 min, 30 min, 45 min, 1 h, 2 h, 4 h, 8 h, 12 h, and 24 h), blood samples were collected from tail vein of rats. The blood samples were placed in a centrifuge tube and anticoagulated with heparin. After centrifugation, the upper plasma was extracted. The rats were sacrificed by dislocation after blood collection. The heart, liver, spleen, lung, kidney, brain, and other tissues were quickly removed, rinsed with normal saline twice and then dried with clean filter paper, which was placed in an AL204 electronic balance (Mettler-Toledo Instruments Ltd., Switzerland) for precise weighing. The above samples were stored in a −20°C refrigerator.

After thawing on the day of measurement, animal organs at each time point were collected, accurately weighed, placed in 10 mL test tubes (BrandTech Scientific, Germany), supplemented with a specified volume of normal saline (Sichuan Kelun Pharmaceutical Co., Ltd., China), and homogenized using a DR25 light electric tissue homogenizer (DISRAD, USA) to obtain tissue homogenates. Then, 500 μL of the latter was accurately weighed, and 2.0 mL methanol (Hangzhou Fine Chemical Co., Ltd., China) was applied in the plate. The plate was oscillated fully by a vortex mixer (Thermo Fisher Scientific, USA) and sonicated (Ultrasonic Systems, Inc., USA) for 2 min.The supernatant was placed in a centrifuge tube (Thermo Fisher Scientific, USA) in a water bath (Thermo Fisher Scientific, USA) after centrifugation and then dried with

N_2 (Guangdong Chinese Academy of Sciences Nitrogen Company, China). The plate was reconstituted with 0.5 mL methanol (Tedia, USA). Centrifugation was performed using the GL-20G-II high-speed refrigerated centrifuge (Shanghai Anting Scientific Instrument Factory, China) at 4°C. A 20 µL aliquot of supernatant was regarded as the sample for determining the concentration of PARI in rat plasma, heart, spleen, liver, lungs, kidneys, and brain.

Targeting evaluation based on sampling of each organ: The drug concentration in each organ and plasma was determined. The imperative index for evaluating targeted preparations was employed to assess the *in vivo* targeting of drugs to specific tissues. In this study, a standard injection of PARI was used as the reference, and targeting parameters such as the total targeting coefficient, relative uptake rate, and peak concentration ratio were calculated to evaluate the targeting efficiency of PARI-BCA-NPs in brain tissue.

Specimen collection and index detection based on each rat model grouping: A global cerebral IRI model was established and assigned into three groups (each group consisted of 18 rats). After 72 h of spontaneous recovery cycle, brain tissues of each group were taken, fixed with 4% paraformaldehyde (Sigma-Aldrich, USA), and stored at −80°C. Prepared paraffin sections were baked in the oven (Thermo Fisher Scientific, USA) and then transferred to xylene (Sigma-Aldrich, USA) for paraffin dissolution, 15 min each time, three times. Then, ethanol (Sigma-Aldrich, USA) dehydration was performed in a concentration gradient (100%, 95%, 90%, 80%, 70%). After the sections were washed with tap water, they were placed in 5% sodium citrate solution (Sigma-Aldrich, USA) for antigen repair under high pressure and then cooled naturally.

Then, 3% hydrogen peroxide (Sigma-Aldrich, USA) was applied dropwise to remove endogenous peroxidase, which was incubated with anti-superoxide dismutase (SOD)1 and anti-SOD2 primary antibodies (ab13498, ab13534, Abcam, UK) and placed in a refrigerator at 4°C overnight. After washing with phosphate buffer saline (PBS) (Thermo Fisher Scientific, USA) for three times, IgG H&L secondary antibody (Alexa Fluor® 647, Abcam, UK) was utilized for incubation and incubated in an incubator at 37°C for 1 h. PBS washing was continued for 5 min each time. The nuclei were stained with 2-(4-Amidinophenyl)-6-indolecarbamidine dihydrochloride (DAPI, Thermo Fisher, USA) for 2 min and then washed with PBS solution for 5 min. Fluorescence images from five different fields were captured using an LSM880 NLO confocal two-photon microscope (Carl Zeiss, Germany) after the sections were sealed with an appropriate amount of anti-fluorescence quenching mounting medium. Care was taken to avoid capturing autofluorescence at the edges of the sections during imaging.

Detection of brain cell apoptosis by Caspase3/TUNEL double labeling: After dewaxing the paraffin sections, antigen retrieval was performed to repair the tissue and eliminate endogenous peroxidase activity. The sections were then incubated with anti-Caspase-3 primary antibody (ab32351, Abcam, UK), which was applied dropwise and incubated at 4°C overnight (Thermo Fisher Scientific, USA). PBS washing lasted for 5 min each time. Secondary antibodies (A02110-1, Abbkine, USA) were applied dropwise for incubation and then placed in an incubator (Thermo Fisher Scientific, USA) for incubation for 1 h at 37°C under dark conditions. Fifty microliters of TUNEL reaction mixture (Roche, Germany) were applied dropwise to each group of slides after they were dried. The slides were then incubated at 37°C for 30 minutes, followed by rinsing with PBS. After drying, DAPI was applied for staining at room temperature, and the slides were subsequently rinsed with PBS. Anti-fluorescence sealing tablets (Thermo Fisher Scientific, USA) were applied dropwise for sealing after the slides were spin-dried. Under a 200× IXplore Pro light microscope (Olympus Corporation, Japan), the sections from various groups were photographed from five positive fields. The apoptosis rate was calculated based on the ratio of Caspase-3/TUNEL-positive cells to the total number of cells in the high-power field.

Statistical methods: The DAS 2.0 pharmacokinetic processing program was utilized to process the drug concentration data of PARI and PARI-BCA-NPs for injection in blood and different tissues after intravenous administration. Data were denoted as the mean plus or minus standard deviation, and a *t* test was conducted among groups, where $P<0.05$ and $P<0.01$ indicated that the differences between the data had statistical significance and significant statistical significance, respectively.

RESULTS

Physical characterization of PARI-BCA-NPs: Figure 1 shows that PARI-BCA-NPs exhibited good dispersibility and no adhesion between the particles, as visualized by transmission electron microscopy. PARI-BCA-NPs prepared in Figure 2 had a mean particle size of 163.8 nm, a uniform size, and a dispersion coefficient of 0.136, which met expectations. NPs with a size range of 100-200 nm can remain in the bloodstream for an extended period and effectively cross cell membranes, enhancing cellular drug uptake. Meanwhile, the smaller particle size contributes to improved drug accumulation in target tissues, particularly in diseased tissues such as tumors. A dispersion index of 0.136 indicates a relatively uniform particle size distribution, which is crucial for ensuring the consistency and reproducibility of the NPs, thereby

aiding in achieving the desired therapeutic efficacy and treatment outcomes (Thapa *et al,* 2021). The DSC results of the PARI parent drug (Figure 3(C)), the blank NPs (Figure 3(B)), and PARI-BCA-NPs (Figure 3(A)) showed that PARI had a very broad absorption peak near 118.3°C. However, there was no peak on the DSC chromatograms of the blank NPs and PARI-BCA-NPs at the corresponding temperature, indicating that PARI existed in the amorphous state of PARI-BCA-NPs. The blank NPs exhibited an absorption peak at 58°C, while the DSC profile of PARI-BCA-NPs showed a rightward shift.

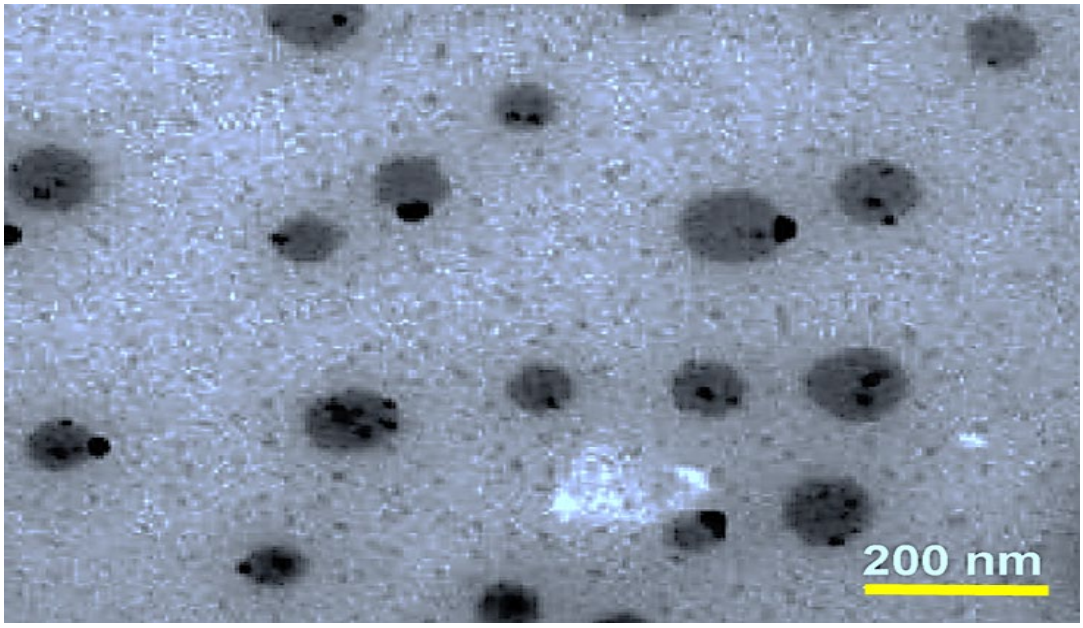

Fig. 1. Transmission electron microscope observation of PARI-BCA-NPs.

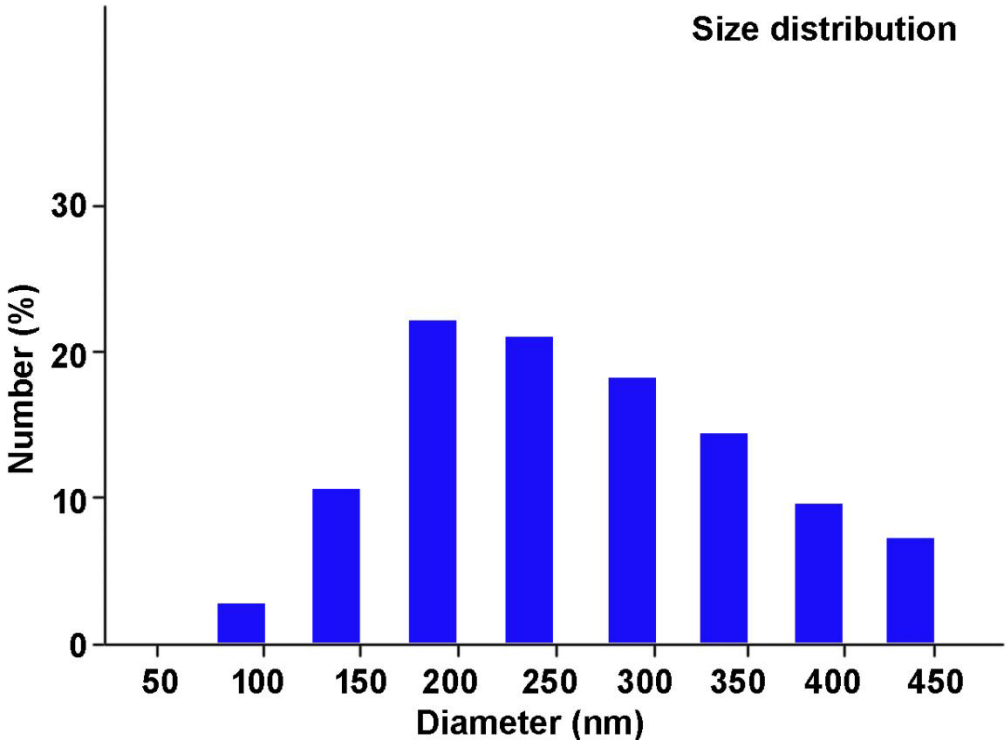

Fig. 2. Particle size distribution of PARI-BCA-NPs.

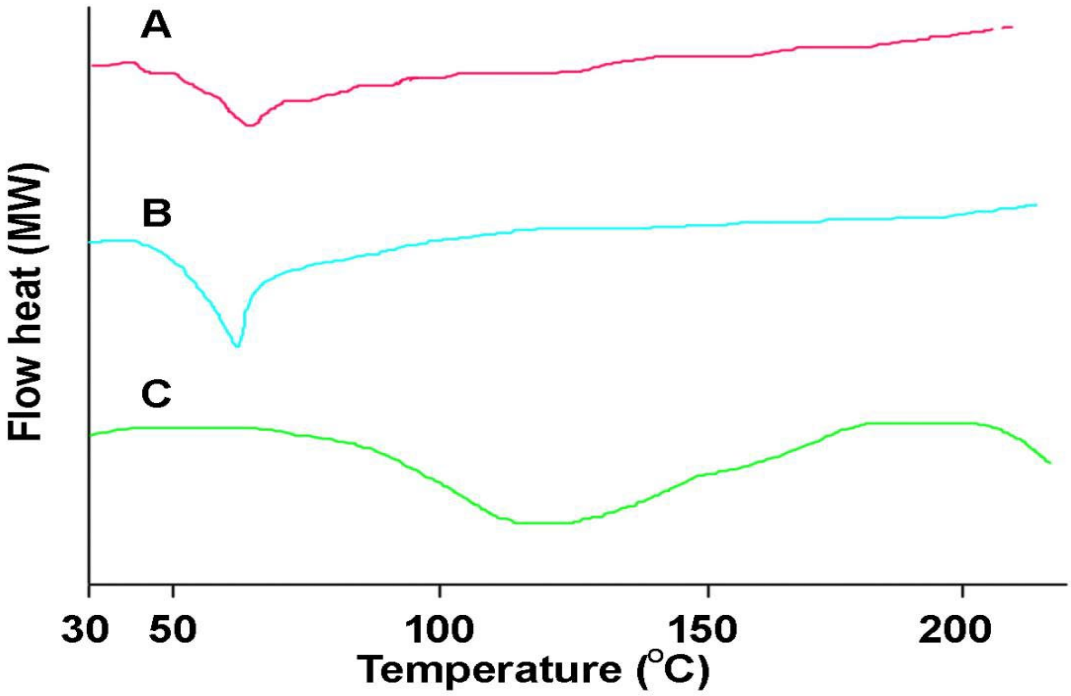

Fig. 3. Differential thermal analysis plot of (A) PARI-BCA-NPs, (B) Blank NPs, (C) PARI parent drug.

The composition of the BCA monomer (Figure 4A), the blank NPs (Figure 4B), PARI-BCA-NPs (Figure 4C), and the PARI parent drug (Figure 4D) was analyzed by Fourier transform infrared spectroscopy (FTIR). Peak at 2,200 cm^{-1} represented a C≡N characteristic peak of the BCA monomer (Figure 4A), which also appeared in the blank NPs (Figure 4B) and PARI-BCA-NPs (Figure 4C). The peak of the blank NPs, PARI-BCA-NPs, and PARI parent drug (Figure 4D) near 3,368 cm^{-1} was −OH, but this peak did not appear in the FTIR spectrum of the BCA monomer. Benzene ring absorption peaks near 650 nm^{-1} and 1,400 nm^{-1} in the PARI chromatogram were also present in the PARI-BCA-NP chromatogram, but the peak intensity was markedly weakened.

Tissue distribution and pharmacokinetic index test of PARI-BCA-NPs in intravenous administration: Figure 5 and Figure 6 show the drug content statistics of PARI-BCA-NPs in brain tissues at various time points, and the change curves of drug concentration after PARI and PARI-BCA-NPs were injected into various tissues at various time points. In Fig.6, the blood drug concentration rapidly decreased after injection of PARI, and the drug was rapidly distributed to various tissues and organs. PARI-BCA-NPs greatly prolonged the retention time of the drug in various tissues. Comparison of the drug content in brain tissue at various time points revealed that, compared to PARI, tail vein injection of PARI-BCA-NPs significantly increased the drug concentration in brain tissue (P<0.05) (Fig.5).

Te indicates that in contrast to the difference in tropism of the same pharmaceutical preparation for various tissues *in vivo*, the larger *Te* was, the more selective the tissue would be. In Figure 7 (A and B), its effects on *Te* in plasma, heart, lung, kidney, and brain increased from 10.38%, 1.26%, 5.37%, 37.8%, and 0.16% of the parent drug to 14.33%, 2.68%, 9.58%, 41.88%, and 0.57%, respectively, after intravenous administration of PARI-BCA-NPs, while those in spleen and liver decreased from 8.69% and 35.74% to 8.36% and 22.43%, respectively (P<0.05). That was, the injection of PARI in NP form into the body would increase the drug concentrations in the heart, lungs, kidneys, and brain.

After intravenous injection of the PARI parent drug and PARI-BCA-NPs in rats, injection of PARI-BCA-NPs resulted in a significant increase in the mean blood drug concentration, compared to the PARI parent drug (Figure 8(A)), drug-time curve area in injected solvent (Figure 8(B)), mean retention time (Figure 8(C)), biological half-life (Figure 8(D)), and maximum blood drug concentration (Figure 8(F)) (P<0.01). There was also a drastic decrease in drug clearance (Figure 8(E)).

The mechanism of PARI-BCA-NPs in the apoptosis of brain cells in CA/CPR: Fluorescence density of SOD1 in each group after 72 h of feeding was compared. In contrast to the sham operation group, fluorescence density of SOD1 in the model group was greatly reduced (P<0.05). Fluorescence density of SOD1 in the PARI-BCA-NP group at 72 h was markedly increased versus that in the model group (P<0.05) (Figure 9).

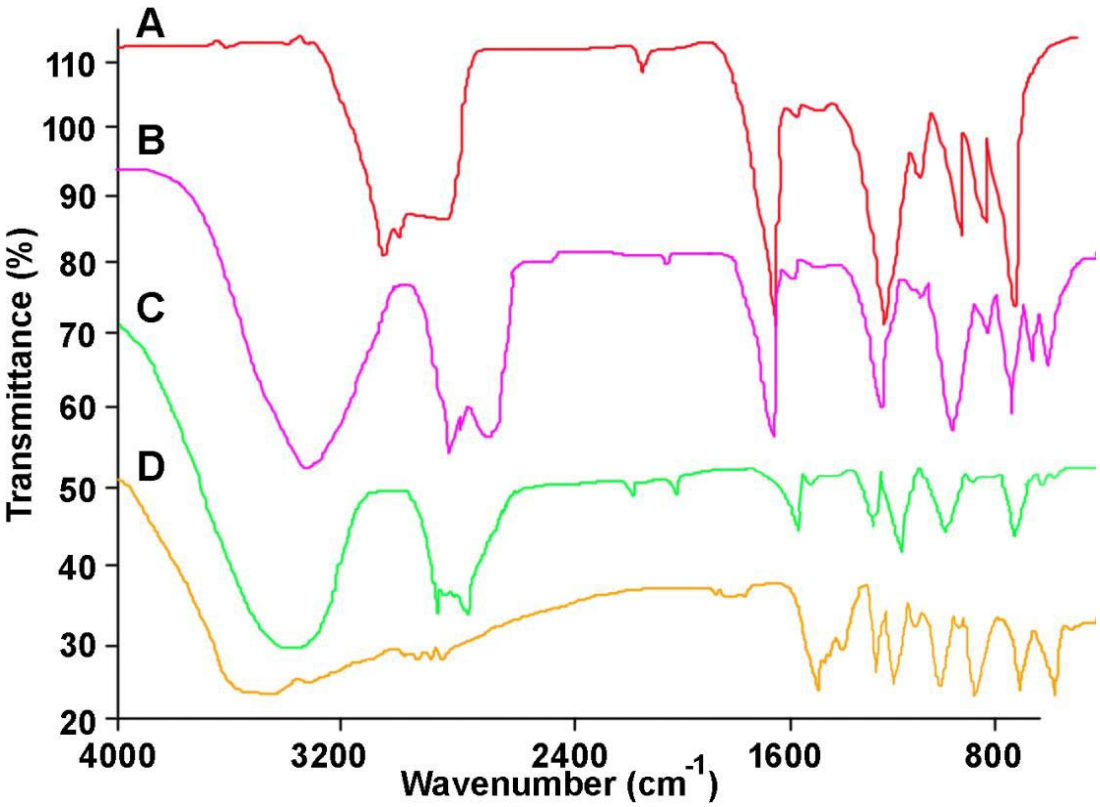

Fig.4. Infrared spectra of various materials. A: BCA monomer; B: blank NPs; C: PARI-BCA-NPs; D: PARI prod rugs.

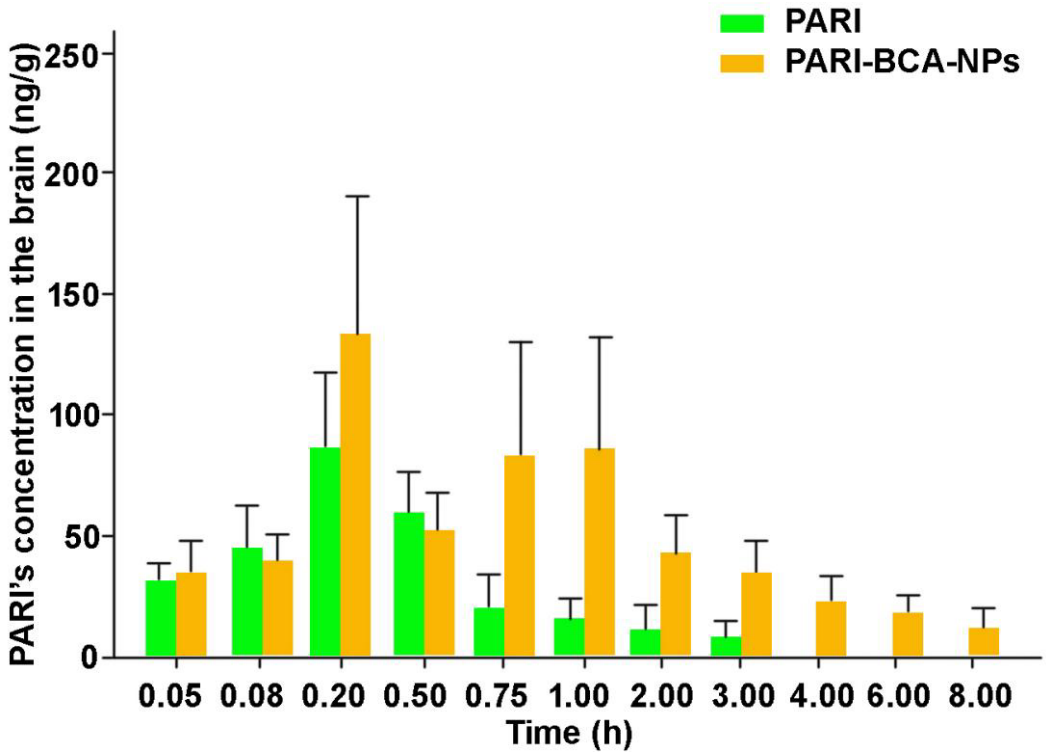

Fig.5. PARI content in brain tissue at each time points after intravenous injection of PARI or PARI-BCA-NPs.

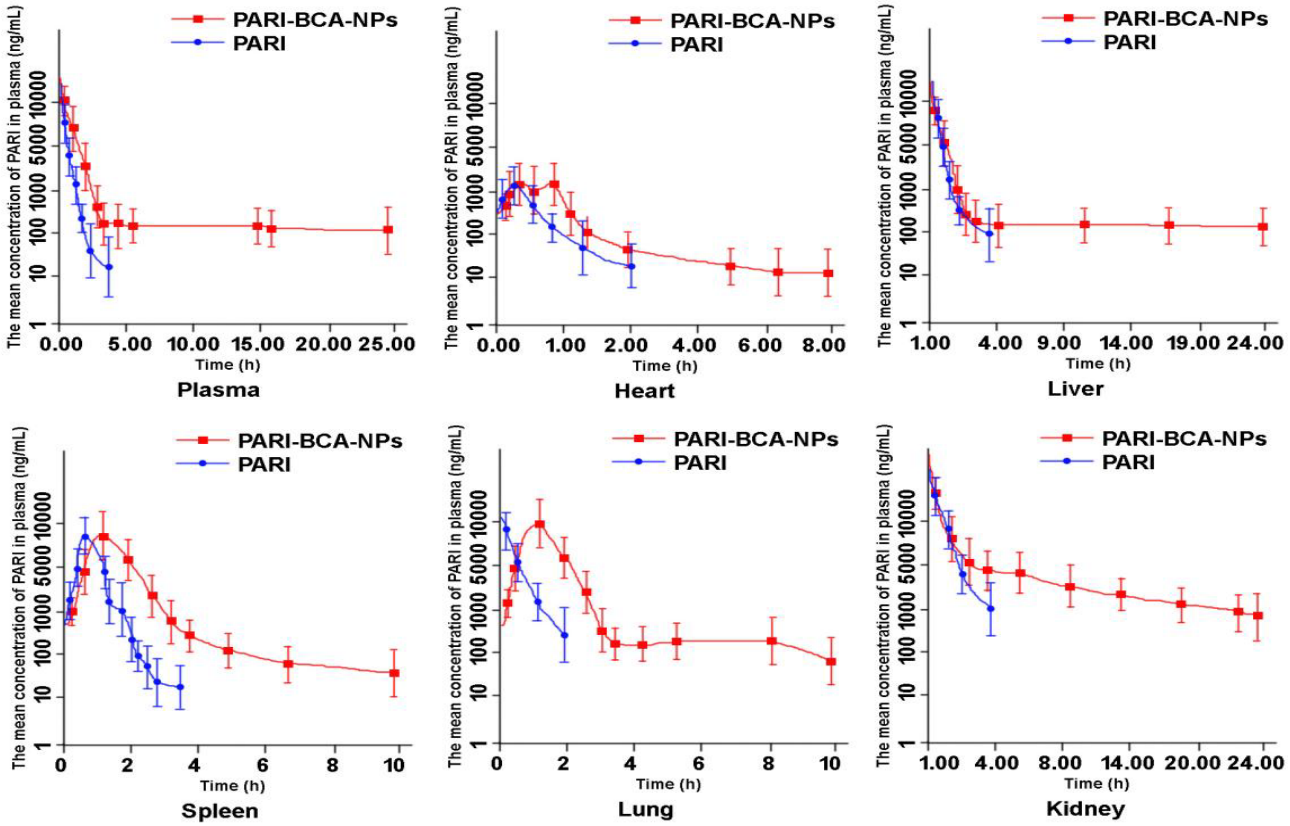

Fig.6. Mean drug concentration-time curves in plasma and tissues after intravenous injection of PARI and PARI-BCA-NPs in rats.

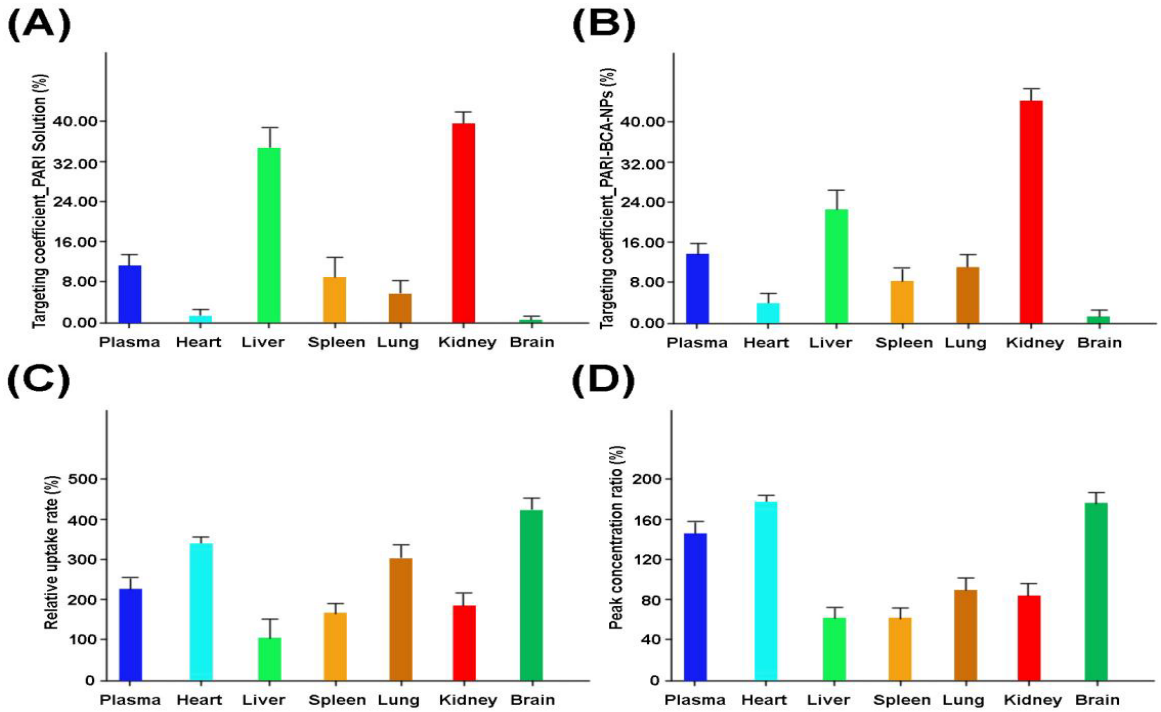

Fig.7. (A) The targeting coefficient of PARI parent drug solution in various tissues, (B) the targeting coefficient of PARI-BCA-NPs in various tissues, (C) the relative uptake rates in various tissues, and (D) the comparison of peak concentrations in various tissues.

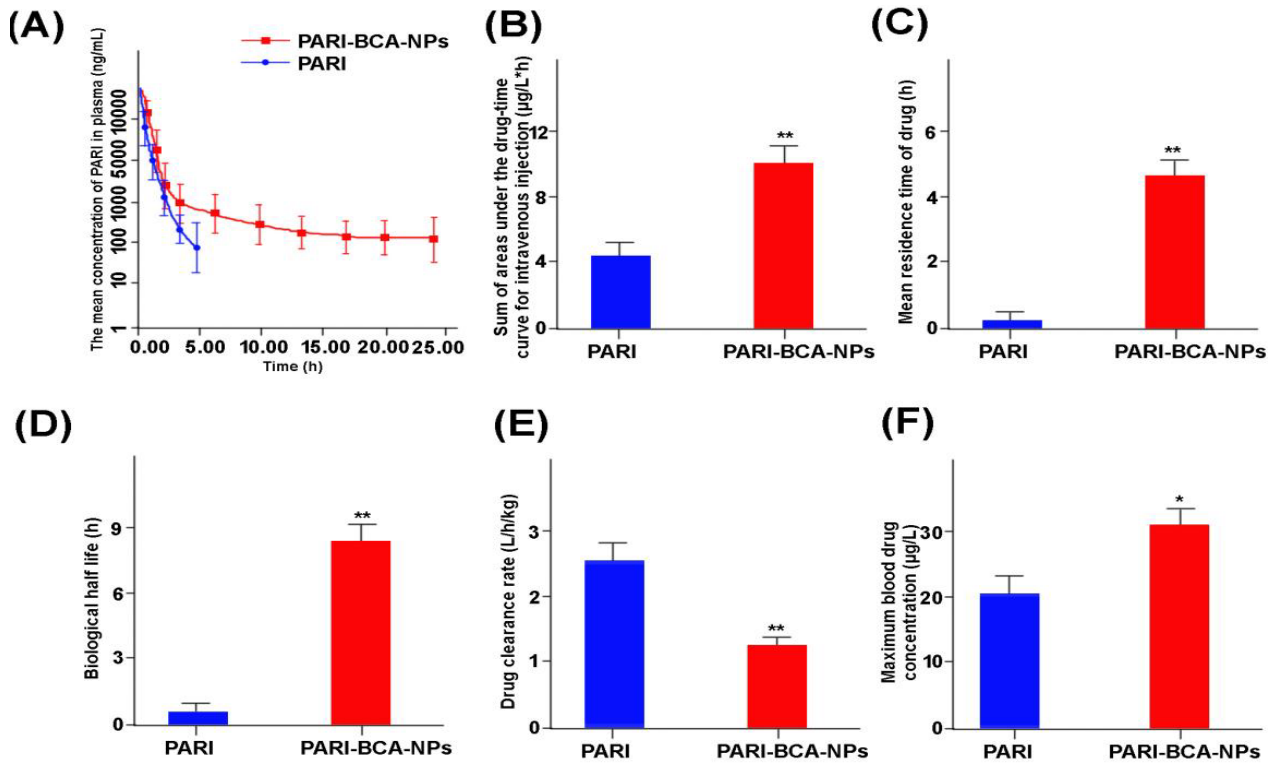

Fig.8. (A) Mean blood drug concentration-time curve of rats after tail vein injection of various solvents, (B) drug-time area curve of different solvents during intravenous injection, (C) mean retention time comparison of various solvents after intravenous injection, (D) biological half-life comparison of various solvents after intravenous injection, (E) drug clearance comparison, and (F) maximum blood drug concentration comparison. Compared with PARI parent drug, *P<0.05, **P<0.01.

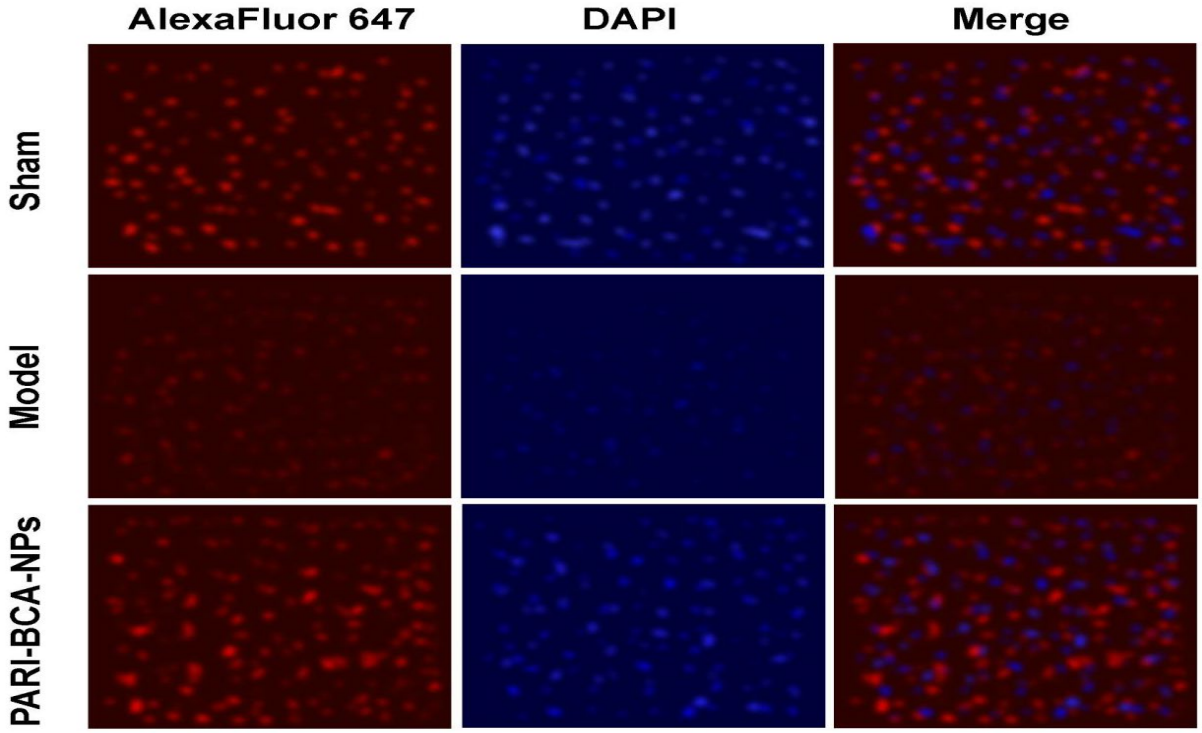

Fig.9. Fluorescence staining results of SOD1 in brain tissue of each group at 72 h of CPR.

In Figure 10, the SOD2 fluorescence intensity of each group was compared. Fluorescence intensity of the PARI-BCA-NPs group was greatly stronger than that of the model group and sham operation group (P<0.05). Fluorescence intensity of the model group was stronger than that of the sham operation group (P<0.05). In Figure 11, the Caspase3/TUNEL and TUNEL-positive rates of brain cells in the administration group at 72 h were lower than those in the model group (P<0.01).

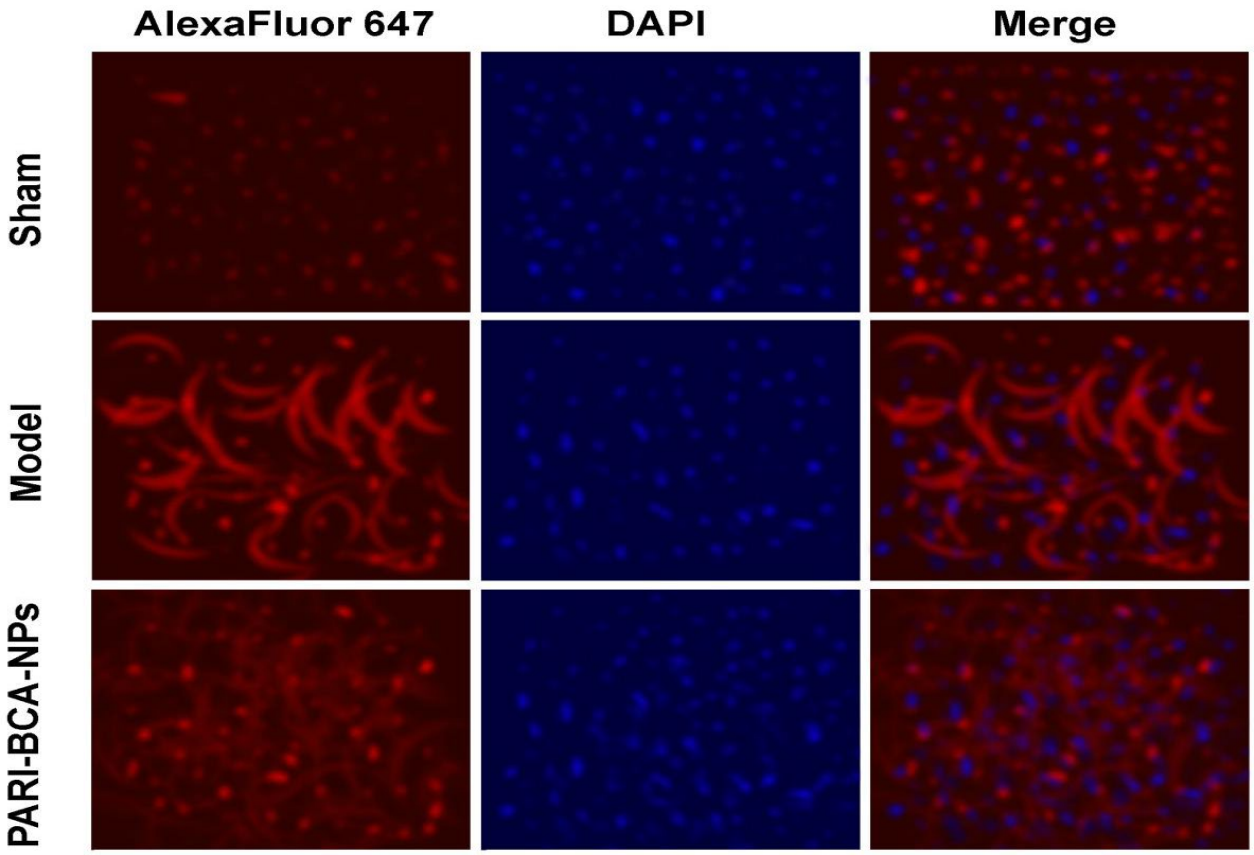

Fig.10. Fluorescence staining results of SOD2 in brain tissue of each group at 72 h of CPR.

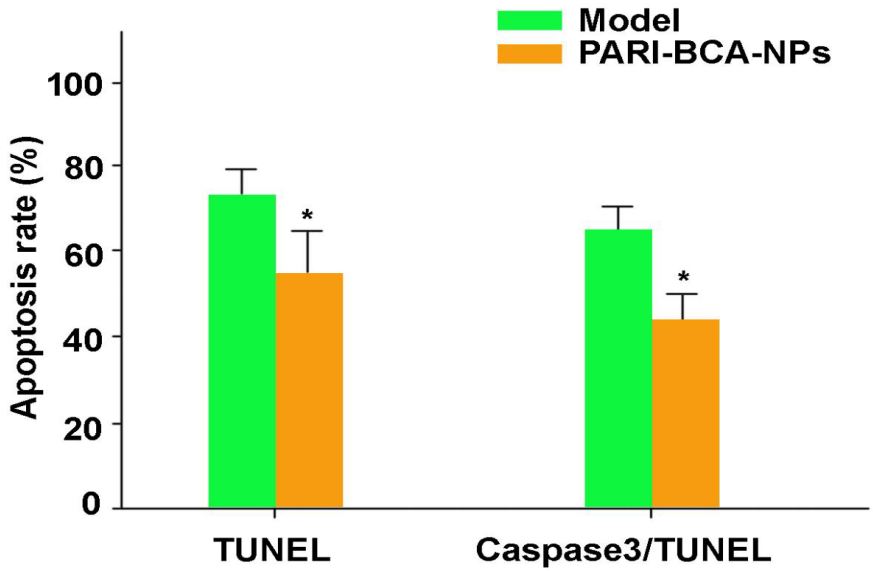

Fig.11. Comparison of the apoptosis rates of brain cells in the model group and the administration group at 72 h. **P*<0.05, ***P*<0.01 vs. model group.

DISCUSSION

This study evaluated the potential of PARI-BCA-NPs in the treatment of post-CA brain injury, with a focus on analyzing the drug targeting ability, antioxidant effects, and apoptosis inhibition. By comparing with existing studies, the advantages and limitations of PARI-BCA-NPs were analyzed, and future research directions were proposed.

PARI-BCA-NPs, as a NP drug carrier, demonstrate significant advantages in improving drug targeting and bioavailability. Compared to PARI, PARI-BCA-NPs show a significantly prolonged retention time in various tissues, particularly resulting in a notable increase in drug concentration in the brain tissue. A study by Singh *et al*. (2013) found that PARI-loaded gold NPs can enhance the drug concentration in brain tissue, indicating that NP carriers help to improve the targeted delivery of drugs to the brain (Singh *et al.,* 2013). Therefore, PARI-BCA-NPs hold promise as an effective drug delivery system in clinical applications, especially for the treatment of brain injuries. However, although current research shows that NP carriers can significantly improve drug targeting, their clinical efficacy in meeting therapeutic needs still requires further validation. The surface characteristics of the NP carrier, the physicochemical properties of the drug, and the chemical stability of the carrier may all influence its targeting ability and drug release efficacy (Matlou *et al.,* 2021; Zhang *et al.,* 2022). Future research should further optimize these factors to ensure their effectiveness in clinical applications.

Furthermore, this study found that PARI-BCA-NPs significantly increased the expression of SOD in brain tissue, enhancing the brain's antioxidant capacity. This result is consistent with the findings of Hu *et al*. (2020), who demonstrated that green tea polyphenols enhanced the endogenous antioxidant capacity of rats by upregulating the expression of SOD1 and SOD2 (Hu *et al.,* 2020). The antioxidant effect of PARI-BCA-NPs may alleviate brain injury induced by oxidative stress by increasing SOD activity (He *et al.,* 2020; Wang *et al.,* 2022; Wang *et al*., 2020). However, although SOD is one of the key antioxidant enzymes, the occurrence of oxidative stress is a complex biological process involving various redox reactions and the generation of free radicals. Therefore, future research should focus more on the role of PARI-BCA-NPs in regulating multiple oxidative stress biomarkers, including ROS generation and the activity of other antioxidant enzymes (Nguyen *et al.,* 2020; Subramanian *et al.,* 2022).

In terms of apoptosis, PARI-BCA-NPs significantly reduced the ratio of Caspase-3 and TUNEL-positive cells in brain tissue, indicating that the drug effectively inhibits cell apoptosis. Consistent with the studies by Rogers *et al*. (2019) and Unnisa *et al*. (2023), Caspase-3, as a key protein in apoptosis, plays a crucial role in reducing cell death induced by oxidative stress, thereby alleviating brain injury (Rogers *et al.,* 2019; Unnisa *et al.,* 2023). The results from the TUNEL assay and Caspase-3 expression suggest that PARI-BCA-NPs exert a protective effect by inhibiting Caspase-3 activation, thus reducing neuronal apoptosis. This mechanism provides a molecular basis for the application of PARI-BCA-NPs in the treatment of brain injury. However, despite Caspase-3 inhibition being central to apoptosis, PARI-BCA-NPs may regulate cell death through multiple signaling pathways, such as NF-κB, p53, and others. Therefore, future research should further investigate whether PARI-BCA-NPs alleviate brain injury through a synergistic effect of multiple pathways.

In terms of pharmacokinetics, this study found significant changes in the pharmacokinetic parameters of PARI-BCA-NPs following intravenous injection. Compared to PARI, their half-life, retention time, and maximum blood drug concentration were all significantly increased, while the drug clearance rate was notably decreased. This indicates that PARI-BCA-NPs can prolong the retention time of the drug in the body, thereby enhancing its therapeutic efficacy. A study by Song *et al*. (2024) also demonstrated that NP carriers can improve the distribution and retention time of drugs in the body, thereby enhancing their therapeutic effects (Song *et al.,* 2024). These findings provide strong support for the application of PARI-BCA-NPs in the treatment of brain injury. However, pharmacokinetic changes are influenced by multiple factors, including the degradation properties of the drug, the structural stability of the carrier, and differences in animal models. Therefore, although this study shows that PARI-BCA-NPs have a longer retention time, future research should continue to assess the performance of these drugs in clinical settings, particularly regarding drug metabolism and clearance under different disease conditions.

Although this study demonstrates the potential of PARI-BCA-NPs in the treatment of post-CA brain injury, certain limitations remain. First, the study was primarily conducted in animal models, and long-term follow-up data and clinical validation are still lacking. Therefore, whether these findings can be effectively translated into clinical treatment requires further preclinical and clinical research. Second, while the changes in pharmacokinetic parameters suggest the superiority of PARI-BCA-NPs in the body, their performance may vary across different individuals. Future studies should focus on personalized treatment and the variability in drug response. Additionally, although this study primarily assessed the effects of PARI-BCA-NPs on antioxidant and anti-apoptotic mechanisms, further exploration is needed to understand their impact on other mechanisms of brain injury, such as inflammation and neuroprotection. The potential toxicity,

long-term accumulation effects, and impacts on other biological systems of the NP carriers also warrant further attention in future research.

Conclusion: PARI was utilized as a model drug to prepare PARI-BCA-NPs, and alongside characterization analysis, pharmacokinetics after intravenous administration and tissue distribution *in vivo* were investigated. Subsequently, a rat CA/CPR model was established to demonstrate protective effect of the nanocarrier drug on brain cells. PARI-BCA-NPs significantly prolonged the retention time of the drug in various tissues and further reduced the apoptosis rate of brain cells 72 hours after CPR by promoting the expression of SOD in brain tissue. However, this study has certain limitations. It only analyzed the effects of PARI-BCA-NPs on CA/CPR rats without comparing them to other therapeutic drugs. Additionally, the impact of PARI-BCA-NPs on rat cardiac function was not evaluated. Therefore, further refinement of the experimental design is needed in future studies to investigate the potential mechanisms underlying PARI-BCA-NPs therapy for CA/CPR. Overall, the findings of this study have significant implications for CA/CPR treatment and contribute to the enhancement of drug efficacy.

Abbreviations: PARI: Puerarin; BCA: polybutyl cyanoacrylate; NPs: nanoparticles; CA: cardiac arrest; CPR: cardiopulmonary resuscitation; DSC: differential scanning calorimetry; AUC: area under curve; SOD: superoxide dismutase; IRI: ischemia–reperfusion injury; PBS: phosphate buffer saline; DAPI: 2-(4-Amidinophenyl)-6-indolecarbamidine dihydrochloride.

Author's contribution: Conception and study design: Xue Zhao; data acquisition and analysis: Yuanshen Xu and Jinyan Fang; manuscript draft, editing and revision: Xue Zhao. All authors wrote and approved the final manuscript.

Availability of Data and Material: All data generated during this study are included in this published article.

Declaration of Conflicting Interests: The authors declared no potential conflicts of interest with respect to the research, authorship, and/or publication of this article.

Animal Ethics: All animal experiments were approved by the Animal Ethics Committee of Affiliated Hangzhou First People's Hospital, in compliance with Chinese national guidelines for the care and use of animals.

Funding: This work was supported by The Medical and Health Research Project of Zhejiang Province (Grant: 2023KY924) and The Construction Fund of Medical Key Disciplines of Hangzhou (Grant: OO20200485).

REFERENCES

Chen, Z.Q., Y. Zhou, J.W. Huang, F. Chen, J. Zheng, H.L. Li, T. Li and L. Li (2021). Puerarin pretreatment attenuates cardiomyocyte apoptosis induced by coronary microembolization in rats by activating the PI3K/Akt/GSK-3β signaling pathway. Korean J Physiol Pharmacol, 25(2), 147–157. https://doi.org/10.4196/kjpp.2021.25.2.147

Cheng, J., H. Yu, Z.F. Zhang, H.X. Jiang, P. Wu, Z.G. Wang, Z.B. Chen and L.Q. Wu (2024). Mxene-bpV plays a neuroprotective role in cerebral ischemia-reperfusion injury by activating the Akt and promoting the M2 microglial polarization signaling pathways. J Mater Sci Mater Med, 35(1), 42. https://doi.org/10.1007/s10856-024-06811-0

Ferraris, C., R. Cavalli, P.P. Panciani and L. Battaglia (2020). Overcoming the blood-brain barrier: successes and challenges in developing nanoparticle-mediated drug delivery systems for the treatment of brain tumours. Int J Nanomedicine, 15, 2999–3022. https://doi.org/10.2147/IJN.S231479

Gvoic, M., S. Vukmirovic, H. Al-Salami, A. Mooranian, M. Mikov and K. Stankov (2021). Bile acids as novel enhancers of CNS targeting antitumor drugs: a comprehensive review. Pharm Dev Technol, 26(6), 617–633. https://doi.org/10.1080/10837450.2021.1916032

He, Y., B. Liu, P. Yao, Y. Shao, Y. Cheng, J. Zhao, J. Wu, Z.W. Zhao, W. Huang, T.A. Christopher, B. Lopez, X. Ma and Y. Cao (2020). Adiponectin inhibits cardiac arrest/cardiopulmonary resuscitation-induced apoptosis in brain by increasing autophagy involved in AdipoR1-AMPK signaling. Mol Med Rep, 22(2), 870–878. https://doi.org/10.3892/mmr.2020.11181

Hoffmann, M., N. Hersch, R. Merkel, A. Csiszar and B. Hoffmann. (2019). Changing the way of entrance: highly efficient transfer of mRNA and siRNA via fusogenic nano-carriers. J Biomed Nanotechnol, 15(1), 170–183. https://doi.org/10.1166/jbn.2019.2663

Hu, W., H. Wang, Q. Shu, M. Chen and L. Xie (2020). Green tea polyphenols modulated cerebral SOD expression and endoplasmic reticulum stress in cardiac arrest/cardiopulmonary resuscitation rats. Biomed Res Int, 2020, 5080832. https://doi.org/10.1155/2020/5080832

Jahansooz, F., B.E. Hosseinzade, A.H. Zarmi, F. Hadi, S.M. Massood Hojjati and K. Shahpasand (2020). Dopamine-loaded poly (butyl cyanoacrylate) nanoparticles reverse behavioral deficits in Parkinson's animal models. Ther Deliv, 11(6), 387–399. https://doi.org/10.4155/tde-2020-0026

Lott, C., A. Truhlář, A. Alfonzo, A. Barelli, V. González-Salvado, J. Hinkelbein, J.P. Nolan, P. Paal, G.D.

Perkins, K.C. Thies, J. Yeung, D.A. Zideman, J. Soar and ERC Special Circumstances Writing Group Collaborators (2021). European Resuscitation Council guidelines 2021: cardiac arrest in special circumstances. Resuscitation, 161, 152–219. https://doi.org/10.1016/j.resuscitation.2021.02.011

Ma, Q., D. Liu, R. Gong, S. Chen, F. Fang and Y. Zhuang (2021). Mechanically induced vasospasm-evaluation of spasmolytic efficacy of 10 pharmaceutical agents using laser speckle contrast imaging. Lasers Surg Med, 53(5), 684-694. https://doi.org/10.1002/lsm.23347.

Matalqah, S.M., K. Aiedeh, N.M. Mhaidat, K.H. Alzoubi, Y. Bustanji and I. Hamad (2020). Chitosan nanoparticles as a novel drug delivery system: a review article. Curr Drug Targets, 21(15), 1613–1624. https://doi.org/10.2174/1389450121666200711172536

Matlou, G.G. and H. Abrahamse (2021). Hybrid inorganic-organic core-shell nanodrug systems in targeted photodynamic therapy of cancer. Pharmaceutics, 13(11), 1773. https://doi.org/10.3390/pharmaceutics13111773

Masoudi Asil, S., J. Ahlawat, G. Guillama Barroso and M. Narayan (2020). Nanomaterial based drug delivery systems for the treatment of neurodegenerative diseases. Biomater Sci, 8(15), 4109–4128. https://doi.org/10.1039/d0bm00809e

Mitchell, M.J., M.M. Billingsley, R.M. Haley, M.E. Wechsler, N.A. Peppas and R. Langer (2021). Engineering precision nanoparticles for drug delivery. Nat Rev Drug Discov, 20(2), 101–124. https://doi.org/10.1038/s41573-020-0090-8

Nguyen, V.T.T., N. Darville and A. Vermeulen (2022). Pharmacokinetics of long-acting aqueous nano-/microsuspensions after intramuscular administration in different animal species and humans: a review. AAPS J, 25(1), 4. https://doi.org/10.1208/s12248-022-00771-5

Reker, D., Y. Rybakova, A.R. Kirtane, R. Cao, J.W. Yang, N. Navamajiti, A. Gardner, R.M. Zhang, T. Esfandiary, J. L'Heureux, T. von Erlach, E.M. Smekalova, D. Leboeuf, K. Hess, A. Lopes, J. Rogner, J. Collins, S.M. Tamang, K. Ishida, P. Chamberlain, D. Yun, A. Lytton-Jean, C.K. Soule, J.H. Cheah, A.M. Hayward, R. Langer and G. Traverso (2021). Computationally guided high-throughput design of self-assembling drug nanoparticles. Nat Nanotechnol, 16(6), 725–733. https://doi.org/10.1038/s41565-021-00870-y

Rogers, C., D.A. Erkes, A. Nardone, A.E. Aplin, T. Fernandes-Alnemri and E.S. Alnemri (2019). Gasdermin pores permeabilize mitochondria to augment caspase-3 activation during apoptosis and inflammasome activation. Nat Commun, 10(1), 1689. https://doi.org/10.1038/s41467-019-09397-2

Sharma, G., A.R. Sharma, S.S. Lee, M. Bhattacharya, J.S. Nam and C. Chakraborty (2019). Advances in nanocarriers enabled brain targeted drug delivery across blood brain barrier. Int J Pharm, 559, 360–372. https://doi.org/10.1016/j.ijpharm.2019.01.056

Singh, A.K., Y. Jiang, S. Gupta, M. Younus and M. Ramzan (2013). Anti-inflammatory potency of nano-formulated puerarin and curcumin in rats subjected to the lipopolysaccharide-induced inflammation. J Med Food, 16(10), 899–911. https://doi.org/10.1089/jmf.2012.0049

Song, H., C. Guo, Y. Wu, Y. Liu, Q. Kong and Y. Wang (2024). Therapeutic factors and biomaterial-based delivery tools for degenerative intervertebral disc repair. Front Cell Dev Biol, 12, 1286222. https://doi.org/10.3389/fcell.2024.1286222

Sønstevold, T., N. Engedal and M.L. Torgersen (2021). Perturbation of cellular redox homeostasis dictates divergent effects of Polybutyl Cyanoacrylate (PBCA). Nanoparticles on Autophagy. Cells, 10(12), 3432. https://doi.org/10.3390/cells10123432

Subramanian, D.A., R. Langer and G. Traverso (2022). Mucus interaction to improve gastrointestinal retention and pharmacokinetics of orally administered nano-drug delivery systems. J Nanobiotechnology, 20(1), 362. https://doi.org/10.1186/s12951-022-01539-x

Thapa, R., S. Mondal, J. Riikonen, J. Rantanen, S. Näkki, T. Nissinen, A. Närvänen and V.P. Lehto (2021). Biogenic nanoporous silicon carrier improves the efficacy of buparvaquone against resistant visceral leishmaniasis. PLoS Negl Trop Dis, 15(6), e0009533. https://doi.org/10.1371/journal.pntd.0009533

Unnisa, A., N.H. Greig and M.A. Kamal (2023). Inhibition of Caspase 3 and Caspase 9 mediated apoptosis: a multimodal therapeutic target in traumatic brain injury. Curr Neuropharmacol, 21(4), 1001–1012. https://doi.org/10.2174/1570159X20666220327222921

Vimalnath, K.V., A. Rajeswari, S. Patra, K.K. Kamaleshwaran, and S. Chakraborty (2024). Multi-dose formulation and clinical deployment of [Y]Y-labeled hydroxyapatite (HA) microparticles for radiation synovectomy in India- the inherent intricacies. *Appl Radiat Isot*, *217*, 111644. https://doi.org/10.1016/j.apradiso.2024.111644

Wang, J. and M. Zhou (2022). Research progress of S-nitrosoglutathione reductase inhibitors in the regulation of cerebral injury after cardiac arrest-cardiopulmonary resuscitation. Zhonghua Wei Zhong Bing Ji Jiu Yi Xue, 34(9), 995–998. https://doi.org/10.3760/cma.j.cn121430-20210020300198

Wang, S.A., C.P. Su, H.Y. Fan, W.H. Hou and Y.C. Chen (2020). Effects of real-time feedback on cardiopulmonary resuscitation quality on outcomes in adult patients with cardiac arrest: A systematic review and meta-analysis. Resuscitation, 155, 82–90. https://doi.org/10.1016/j.resuscitation.2020.07.024

You, Q., T. Hopf, W. Hintz, S. Rannabauer, N. Voigt, B. van Wachem, P. Henrich-Noack and B.A. Sabel (2019). Major effects on blood-retina barrier passage by minor alterations in design of polybutylcyanoacrylate nanoparticles. J Drug Target, 27(3), 338–346. https://doi.org/10.1080/1061186X.2018.1531416

Zhang, D., L. Liu, J. Wang, H. Zhang, Z. Zhang, G. Xing, X. Wang and M. Liu (2022). Drug-loaded PEG-PLGA nanoparticles for cancer treatment. Front Pharmacol, 13, 990505. https://doi.org/10.3389/fphar.2022.990505

Zhang, S., Q. Ou, P. Xin, Q. Yuan, Y. Wang and J. Wu (2019). Polydopamine/puerarin nanoparticle-incorporated hybrid hydrogels for enhanced wound healing. Biomater Sci, 7(10), 4230–4236. https://doi.org/10.1039/c9bm00991d

Zhou, Y., M. Li, J. Song, Y. Shi, X. Qin, Z. Gao, Y. Lv, and G. Du (2020). The cardioprotective effects of the new crystal form of puerarin in isoproterenol-induced myocardial ischemia rats based on metabolomics. Sci Rep, 10(1), 17787. https://doi.org/10.1038/s41598-020-74246-y.